Water influx is required for CD4$^+$ T cell activation and T cell-dependent antibody responses

Authors:
Joshua Biggs O'May[1], Lesley Vanes[1], Harald Hartweger[1], Leonard L. de Boer[1], Darryl Hayward[1], Robert Köchl[1], Victor L. J. Tybulewicz[1,2]*

Affiliations:
[1]The Francis Crick Institute, London, NW1 1AT, UK
[2]Imperial College, London W12 0NN, UK

*Correspondence to:

Victor L. J. Tybulewicz
The Francis Crick Institute,
1 Midland Road,
London, NW1 1AT, UK

Tel: +44 20 3796 1612
Email: Victor.T@crick.ac.uk

Present addresses:

HH: Laboratory of Molecular Immunology, The Rockefeller University, 10065 New York, NY, USA
DH: GSK, Stevenage, SG1 2NY, UK
RK: Kings College London, London, SE1 9RT, UK

Abstract:

Signaling from the T cell antigen receptor (TCR) on $CD4^+$ T cells triggers the adaptive immune response by inducing T cell activation, proliferation, and differentiation. However, TCR signaling pathways are incompletely understood. Unexpectedly, we demonstrate that WNK1, a kinase previously implicated in osmoregulation in the kidney, is required for T-dependent antibody responses. We show that WNK1-OXSR1-STK39-dependent water influx through AQP3 is required for TCR signaling in $CD4^+$ T cells and for entry into cell cycle. Additionally, by preventing ATR activation this signaling pathway is required for T cells to progress through the G2 phase of the cell cycle. Thus, TCR signaling via WNK1, OXSR1, STK39 and AQP3 leads to water entry that is essential for $CD4^+$ T cell proliferation and hence T cell-dependent antibody responses.

One Sentence Summary:

T cell antigen receptor signaling via the WNK1 kinase causes water entry which is essential for $CD4^+$ T cell proliferation.

Main text:

T cell activation is a critical event in the initiation of T cell-dependent (TD) immune responses. To generate TD antibody responses, naive $CD4^+$ T cells circulate through lymphoid organs searching for antigenic peptides presented on MHC class II molecules (pMHCII) on the surface of antigen-presenting cells (APC) (*1*). Simultaneous binding of cognate pMHCII complexes to the T cell antigen receptor (TCR) and ligation of costimulatory receptors such as CD28 results in biochemical signals leading to LFA-1 integrin-mediated adhesion of the T cell to the APC, and subsequent activation of the T cell characterized by changes in gene expression, cytokine secretion, cell division and differentiation into effector T cells such as T follicular helper (T_{FH}) cells (*2*). T_{FH} cells provide

help to antigen-specific B cells, supporting their activation, proliferation, and differentiation into antibody-secreting plasma cells, thereby delivering an antibody response.

WNK1 has been studied most extensively in the kidney where it acts in epithelial cells of the distal tubules to regulate uptake of ions from urine into the blood stream (*3, 4*). WNK1 phosphorylates and activates OXSR1 and STK39, two related kinases, which in turn phosphorylate members of the SLC12A-family of ion co-transporters, leading to the net influx of Na^+, K^+ and Cl^- ions (*5-8*). Our previous studies in $CD4^+$ T cells showed that WNK1 is rapidly activated by signals from the TCR and CCR7, regulating LFA-1-dependent adhesion as well as CCL21-induced migration through OXSR1, STK39 and SLC12A2 (*9*). Based on these results we hypothesized that WNK1 may be important for TD immune responses.

To investigate this, we reconstituted RAG1-deficient mice with bone marrow from *Wnk1*$^{fl/-}$/RCE mice in which *Wnk1* could be inducibly inactivated in T cells by tamoxifen administration, or with control *Wnk1*$^{fl/+}$/RCE marrow in which *Wnk1* expression was maintained after tamoxifen treatment (Fig. S1A). *Wnk1* was efficiently deleted in $CD4^+$ T cells from these chimeras following tamoxifen administration (Fig. S1B). Using mixed bone marrow chimeras in which *Wnk1* was deleted from all $\alpha\beta$T cells, while other cell types retained *Wnk1* expression, we found that following immunization with NP-CGG in alum, the mice failed to generate NP-specific IgG1 antibodies, a hallmark TD response (Fig. 1A-B). Thus, WNK1 is required in $\alpha\beta$T cells for TD antibody responses.

To identify the WNK1-dependent processes contributing to TD antibody responses, we generated *Wnk1*$^{fl/+}$RCE OT-II and *Wnk1*$^{fl/-}$RCE OT-II bone marrow chimeras which

express a TCR (OT-II) specific for an ovalbumin peptide ($OVA_{323-339}$) presented on the I-A^b MHC class II molecule (*10*). We treated the chimeras with tamoxifen, isolated WNK1-expressing and WNK1-deficient $CD4^+$ OT-II T cells, and transferred these into congenically-marked wild-type (WT) mice which were immunized with ovalbumin (Fig. 1C). Flow cytometric analysis showed that WNK1-deficient OT-II T cells were severely impaired in proliferation at day 3, and at day 7 many fewer WNK1-deficient OT-II T cells were recovered compared to controls, and very few had differentiated into T_{FH} cells (Fig. 1D-J). The almost complete absence of T_{FH} cells likely explains the impaired TD antibody response in mice with WNK1-deficient T cells.

To study this phenotype further, we investigated whether the activation defect of WNK1-deficient T cells could be recapitulated *in vitro*. We cultured WNK1-expressing and WNK1-deficient $CD4^+$ OT-II T cells with bone marrow-derived APCs and different doses of $OVA_{323-339}$ peptide (Fig. S2A). We found that in the absence of WNK1, OT-II T cells were impaired in proliferation, similar to the phenotype observed *in vivo* (Fig. 2A-B). Since in this T cell:APC co-culture assay T cells need to adhere to APCs and receive signals from multiple cell surface proteins in addition to the TCR, we simplified the *in vitro* analysis further by activating purified naive $CD4^+$ T cells with plate-bound anti-CD3ε and anti-CD28 antibodies to stimulate the TCR and CD28 respectively (Fig. S2B). Once again, we found that WNK1-deficient T cells were severely impaired in TCR/CD28-induced proliferation (Fig. 2C-D). This observation suggests that the requirement for WNK1 during $CD4^+$ T cell activation is independent of its role in migration and integrin-mediated adhesion as T cells do not need to migrate or adhere to APCs in order to be activated in this experimental system. Our results show that WNK1 is required for TCR/CD28-induced proliferation, explaining the strongly impaired $CD4^+$ T cell expansion *in vivo* during a TD immune response.

To evaluate the role of WNK1 kinase activity in this process, we analyzed TCR/CD28-induced activation of CD4$^+$ T cells expressing a kinase-inactive allele of WNK1 (*Wnk1*^{D368A}) (Fig. S2B), which again showed strongly decreased cell division, similar to the phenotype of WNK1-deficient T cells (Fig. 2E-F). To address whether the phenotypic changes observed were due to adaptation of cells to the chronic absence of WNK1 activity, rather than a requirement for WNK1 during TCR stimulation, we made use of WNK463 (WNKi), a highly selective WNK kinase inhibitor (*11*). Activation of WT CD4$^+$ T cells in the presence of WNKi showed that inhibition of WNK1, the only WNK-family kinase expressed in T cells, resulted once again in dramatically impaired proliferation upon TCR and CD28 co-stimulation (Figs. S2C, 2G-H). Taken together, these results show that WNK1 kinase activity is required for TCR/CD28-induced proliferation of CD4$^+$ T cells.

The best characterized WNK1 substrates are the related OXSR1 and STK39 kinases (*5-8*). Thus, we investigated if these proteins might be important for WNK1-dependent T cell activation. We again used mice in which *Oxsr1* could be inducibly deleted by tamoxifen treatment. To account for potential redundancy between OXSR1 and STK39, we crossed in the *Stk39*^{T243A} allele which expresses an STK39 mutant that cannot be phosphorylated and activated by WNK1 (*12*). We used bone marrow from *Oxsr1*$^{fl/fl}$*Stk39*$^{T243A/T243A}$RCE as well as control *Oxsr1*$^{+/+}$*Stk39*$^{+/+}$RCE mice to reconstitute irradiated RAG1-deficient mice (Fig. S3A). OXSR1 was efficiently deleted in CD4$^+$ T cells from these chimeras following tamoxifen administration (Fig. S3B). *Oxsr1*$^{-/-}$*Stk39*$^{T243A/T243A}$RCE double mutant CD4$^+$ T cells exhibited reduced TCR/CD28-induced proliferation, however the decrease was smaller than that seen in the absence of WNK1 (Fig. 2I-J). Our results suggest that a WNK1-OXSR1-STK39 pathway is required for CD4$^+$ T cell proliferation.

In kidney epithelial cells, signaling through WNK1, OXSR1 and STK39 leads to phosphorylation of SLC12A-family ion co-transporters and net influx of Na^+, K^+ and Cl^- ions (*6*). Thus, we hypothesized that TCR signaling via the WNK1-OXSR1-STK39-SLC12A pathway is required for T cell activation. Since $CD4^+$ T cells express at least 4 SLC12A-family proteins which are substrates of OXSR1 and STK39 and are likely to have redundant functions, it is impractical to genetically inactivate all of these simultaneously. However, we noted that one of the effects of ion influx into the cell is that the resulting osmotic gradient causes water influx. Indeed, WNK1 has been implicated in the osmoregulation of cells and in modulating cell volume (*13*). Thus, we hypothesized that TCR signaling through WNK1 would result in water influx and that this may be required for T cell activation. In support of this, stimulation of WT naive $CD4^+$ T cells with anti-CD3ε and anti-CD28 resulted in a cell volume increase, whereas WNKi-treated cells were smaller and did not increase in volume to the same extent (Fig. 2K). Thus, WNK1 is required for cell volume increase in response to TCR and CD28 stimulation.

Water entry into mammalian cells is mediated by aquaporins, channels that allow water to passively flow into or out of cells depending on the osmotic gradient. $CD4^+$ T cells predominantly express AQP3, allowing us to use DFP00173, an AQP3 inhibitor (AQP3i) (*14*) to test the requirement for water entry in T cell activation. Notably, treatment of naive $CD4^+$ T cells with AQP3i gave a significant reduction in cell proliferation, similar to that seen in cells with a double mutation in OXSR1 and STK39 (Fig. 2L-M), supporting our hypothesis that TCR signaling through WNK1, OXSR1 and STK39 results in water entry which may be required for proliferation.

To gain a better understanding of how the WNK1 pathway impacts on T cell proliferation, we evaluated how the cells progress through the cell cycle in the absence of WNK1. Ki67

expression is induced as cells progress from G0 to G1 phase of the cell cycle. Following TCR/CD28 stimulation, control WNK1-expressing cells upregulate Ki67 within 48 h of stimulation (Fig. 3A). WNK1-deficient T cells also upregulated Ki67, but did so more slowly, indicating that their entrance into the cell cycle is delayed. Analysis of Ki67+ cells 3 days after the start of TCR/CD28 stimulation showed that a significant fraction of WNK1-deficient cells accumulated in the G2 phase relative to controls (Figs. S4A, 3B-C), suggesting that their reduced rate of proliferation may also be due to slower progression through G2. Furthermore, the rate of incorporation of the nucleoside analog EdU was greatly reduced in WNK1-deficient T cells indicating progression through S phase is also severely hampered in the absence of WNK1 (Fig. 3D-E).

In response to TCR/CD28 co-stimulation, *Oxsr1*$^{-/-}$*Stk39*$^{T243A/T243A}$RCE double mutant T cells also upregulated Ki67 more slowly than control cells, accumulated in S and G2 phases of the cell cycle and had reduced rates of EdU incorporation (Fig. S4B, 3F-J). Thus WNK1, OXSR1 and STK39 are required for CD4^{+} T cells to efficiently exit G0 and progress through S and G2.

Accumulation of cells in G2 could be caused by the triggering of a cell cycle checkpoint, for example through activation of the ATM or ATR kinases in response to DNA damage. Immunoblot analysis of phosphorylated RPA32 (S4/8, p-RPA32) and phosphorylated H2AX (S139, γH2AX), markers of single-stranded and double-stranded DNA damage respectively, showed no significant elevation of either in WNK1-inhibited T cells stimulated through the TCR and CD28 (Fig. S4C-D). However, as expected, both were robustly increased by treatment with hydroxyurea, which causes replication fork stalling and subsequent DNA damage. Since γH2AX is a marker of ATM activity, these results imply

that inhibition of WNK1 does not result in ATM activation. To measure ATR activity, we immunoblotted cell extracts for phosphorylated CHK1 (S345, p-CHK1), a product of ATR activity. Notably, we detected elevated p-CHK1 in TCR/CD28-stimulated WNKi-treated T cells compared to control T cells, which was reduced in cells treated with AZD6738, an ATR inhibitor (ATRi), indicating that ATR activity was increased in the absence of WNK1 activity (Fig. 3K). Extending this analysis, we found a similar increase in ATR activity in TCR/CD28-stimulated *Oxsr1*$^{-/-}$*Stk39*$^{T243A/T243A}$RCE T cells and in AQP3i-treated T cells (Fig. 3K-L). To evaluate if increased ATR activity in WNK1-inihibited T cells was causing cell cycle arrest, we activated WNK1-inihibited T cells and treated them with ATRi. We found that the inhibitor significantly reduced the fraction of cells in G2, implying that the block in G2 is predominantly due to ATR activation (Fig. 3M, S4E). Thus, compromised TCR/CD28 signaling via WNK1, OXSR1, STK39 and AQP3 leads to ATR activation and cell cycle arrest.

The defect in G0 exit in TCR/CD28-stimulated WNK1-deficient T cells could be caused by alterations in early signaling events triggered following engagement of TCR and CD28. Flow cytometric analysis of CD4^{+} T cells stimulated with anti-CD3ε and anti-CD28 antibodies in solution showed that WNK1 inhibition had no effect on the phosphorylation of the CD3ζ component of the TCR (p-CD3ζ), one of the earliest measurable biochemical changes following TCR stimulation (Fig. 4A). As expected, this TCR/CD28-induced increase in p-CD3ζ was blocked by treatment with a SRC kinase inhibitor (SRCi). In contrast, WNKi treatment caused a significant reduction in the phosphorylation of the ZAP70 kinase (p-ZAP70) and the ERK kinases (p-ERK), both of which were also blocked by SRCi (Fig. 4B-C). Moreover, p-ERK was reduced in WNKi-treated CD4^{+} T cells activated by plate-bound anti-CD3ε and anti-CD28 antibodies for 1 h, conditions that result

in biphasic activation of ERK and T cell proliferation (Fig. 4D) (*15*). A similar decrease in TCR/CD28-stimulated p-ERK was also seen in *Oxsr1*$^{-/-}$*Stk39*$^{T243A/T243A}$RCE T cells and in AQP3i-treated T cells, implying that WNK1-OXSR1-STK39 signaling and water entry through AQP3 are required for TCR/CD28-induced p-ERK (Fig. 4D-E).

To directly test whether TCR/CD28 signaling through WNK1 leads to water entry that is required for T cell activation, we stimulated WNK1-deficient CD4$^+$ T cells in hypotonic medium, to force water entry by osmosis. Remarkably, we found that hypotonic medium restored much of the reduced TCR/CD28-stimulated p-ERK in WNK1^{D368A}-expressing T cells, and all of the reduced p-ERK in WNKi-treated T cells as measured 1 h after stimulation (Fig. S5A-B, 4F-G). Furthermore, hypotonic medium also rescued most of the defect in TCR/CD28-induced Ki67 upregulation at 2 d (Fig. S5C, 4H). The effect of hypotonic medium could be due to increased water entry into the cell but could also be caused by the reduced concentration of Na^+ and Cl^- ions in the medium. To distinguish these possibilities, we stimulated the T cells in isotonic medium that had the same reduced concentrations of Na^+ and Cl^- but the osmolarity was made isotonic with L-glucose, an inert osmolyte. Importantly, this isotonic medium with reduced Na^+ and Cl^- concentrations was unable to rescue the TCR/CD28-stimulated p-ERK at 1 h or the induction of Ki67 at 2 d in WNK1-deficient CD4$^+$ T cells (Fig. 4F-H). Thus, the rescue seen with hypotonic medium was due to water entry, not reduced ion concentrations. Taken together, these results demonstrate that TCR/CD28 co-stimulation of CD4$^+$ T cells leads to water entry mediated by the WNK1-OXSR1-STK39-AQP3 signaling pathway, and this is required for TCR/CD28-induced ERK activation and entry into G1 (Fig. 4I).

We show that WNK1 signaling through OXSR1, STK39, and AQP3 plays a central role in T cell proliferation in response to antigen, and thus the generation of a class-switched

antibody response. It is required for entry of naive T cells into G1 and progression through S and G2/M. More specifically, WNK1-dependent water influx, a previously unexplored component of the TCR signaling cascade, is required for TCR-induced ERK signaling and thus entry into G1, a process which is strongly dependent on ERK activation (*16*).

Water entry alters a number of biophysical properties of the cell, which could affect TCR signaling. Water influx increases membrane tension which has been shown to regulate signaling pathways (*17-21*). Water entry also reduces molecular crowding thereby increasing rates of intracellular signaling pathways (*22*), and decreases the viscosity of the cytoplasm, resulting in more rapid assembly of macromolecular structures such as microtubules (*23*). Any or all of these changes could facilitate the assembly of the macromolecular TCR signaling complexes at the immune synapse and subsequent signal transduction (*24*). Similarly, water entry could be required to facilitate the function of the macromolecular replisome complex. Furthermore, entry of water into T cells is required to compensate for the rapid synthesis of macromolecules that accompanies T cell activation and entry into G1 (*25*).

We also show that ATR signaling is sensitive to WNK1-OXSR1-STK39-AQP3-dependent water influx and enforces a cell cycle arrest in G2 in its absence. After 24 h T cell division is no longer dependent on TCR signaling (*26*), however we show that water influx is still required to determine the outcome of a cell fate decision, in this case the transition from G2 to M. Unusually, ATR is activated independently of DNA damage in the absence of WNK1 pathway-dependent water influx, potentially by mechanical stress at the nuclear envelope due to dysregulation of cell volume (*27*). Interestingly, other studies have shown that compromised osmoregulation causes G2 arrest in multiple cell types, including T cells

(*28, 29*). Thus, we may have uncovered an ATR-dependent mechanism for a universal osmotically-sensitive cell cycle checkpoint at G2, a possibility that warrants further study.

In summary, we have shown that TCR signaling via WNK1, OXSR1 and STK39 results in AQP3-dependent water influx, which is required for T cell proliferation, and hence for T-dependent antibody responses. More generally, the broad expression of WNK1 (*30*) suggests that WNK1-dependent water influx may be a common feature of mitogenic pathways in many cell types, both within the immune system and beyond.

References:

1. M. J. Miller, O. Safrina, I. Parker, M. D. Cahalan, Imaging the single cell dynamics of CD4+ T cell activation by dendritic cells in lymph nodes. *J Exp Med* **200**, 847-56 (2004).
2. H. Qi, T follicular helper cells in space-time. *Nat Rev Immunol* **16**, 612-25 (2016).
3. J. A. McCormick, D. H. Ellison, The WNKs: atypical protein kinases with pleiotropic actions. *Physiol. Rev.* **91**, 177-219 (2011).
4. M. Shekarabi, J. Zhang, A. R. Khanna, D. H. Ellison, E. Delpire, K. T. Kahle, WNK Kinase Signaling in Ion Homeostasis and Human Disease. *Cell Metab* **25**, 285-299 (2017).
5. D. R. Alessi, J. Zhang, A. Khanna, T. Hochdorfer, Y. Shang, K. T. Kahle, The WNK-SPAK/OSR1 pathway: master regulator of cation-chloride cotransporters. *Sci Signal* **7**, re3 (2014).
6. J. O. Thastrup, F. H. Rafiqi, A. C. Vitari, E. Pozo-Guisado, M. Deak, Y. Mehellou, D. R. Alessi, SPAK/OSR1 regulate NKCC1 and WNK activity: analysis of WNK isoform interactions and activation by T-loop trans-autophosphorylation. *Biochem. J.* **441**, 325-37 (2012).
7. A. C. Vitari, M. Deak, N. A. Morrice, D. R. Alessi, The WNK1 and WNK4 protein kinases that are mutated in Gordon's hypertension syndrome phosphorylate and activate SPAK and OSR1 protein kinases. *Biochem. J.* **391**, 17-24 (2005).
8. A. C. Vitari, J. Thastrup, F. H. Rafiqi, M. Deak, N. A. Morrice, H. K. Karlsson, D. R. Alessi, Functional interactions of the SPAK/OSR1 kinases with their upstream activator WNK1 and downstream substrate NKCC1. *Biochem. J.* **397**, 223-31 (2006).

9. R. Köchl, F. Thelen, L. Vanes, T. F. Brazao, K. Fountain, J. Xie, C. L. Huang, R. Lyck, J. V. Stein, V. L. Tybulewicz, WNK1 kinase balances T cell adhesion versus migration in vivo. *Nat Immunol* **17**, 1075-83 (2016).

10. M. J. Barnden, J. Allison, W. R. Heath, F. R. Carbone, Defective TCR expression in transgenic mice constructed using cDNA-based alpha- and beta-chain genes under the control of heterologous regulatory elements. *Immunol Cell Biol* **76**, 34-40 (1998).

11. K. Yamada, H. M. Park, D. F. Rigel, K. DiPetrillo, E. J. Whalen, A. Anisowicz, M. Beil, J. Berstler, C. E. Brocklehurst, D. A. Burdick, S. L. Caplan, M. P. Capparelli, G. Chen, W. Chen, B. Dale, L. Deng, F. Fu, N. Hamamatsu, K. Harasaki, T. Herr, P. Hoffmann, Q. Y. Hu, W. J. Huang, N. Idamakanti, H. Imase, Y. Iwaki, M. Jain, J. Jeyaseelan, M. Kato, V. K. Kaushik, D. Kohls, V. Kunjathoor, D. LaSala, J. Lee, J. Liu, Y. Luo, F. Ma, R. Mo, S. Mowbray, M. Mogi, F. Ossola, P. Pandey, S. J. Patel, S. Raghavan, B. Salem, Y. H. Shanado, G. M. Trakshel, G. Turner, H. Wakai, C. Wang, S. Weldon, J. B. Wielicki, X. Xie, L. Xu, Y. I. Yagi, K. Yasoshima, J. Yin, D. Yowe, J. H. Zhang, G. Zheng, L. Monovich, Small-molecule WNK inhibition regulates cardiovascular and renal function. *Nat Chem Biol* **12**, 896-898 (2016).

12. F. H. Rafiqi, A. M. Zuber, M. Glover, C. Richardson, S. Fleming, S. Jovanovic, A. Jovanovic, K. M. O'Shaughnessy, D. R. Alessi, Role of the WNK-activated SPAK kinase in regulating blood pressure. *EMBO Mol Med* **2**, 63-75 (2010).

13. P. de Los Heros, D. Pacheco-Alvarez, G. Gamba, Role of WNK Kinases in the Modulation of Cell Volume. *Curr. Top. Membr.* **81**, 207-235 (2018).

14. Y. Sonntag, P. Gena, A. Maggio, T. Singh, I. Artner, M. K. Oklinski, U. Johanson, P. Kjellbom, J. D. Nieland, S. Nielsen, G. Calamita, M. Rutzler, Identification and characterization of potent and selective aquaporin-3 and aquaporin-7 inhibitors. *J Biol Chem* **294**, 7377-7387 (2019).

15. J. P. Roose, M. Mollenauer, M. Ho, T. Kurosaki, A. Weiss, Unusual interplay of two types of Ras activators, RasGRP and SOS, establishes sensitive and robust Ras activation in lymphocytes. *Mol Cell Biol* **27**, 2732-45 (2007).

16. L. J. Appleman, A. A. van Puijenbroek, K. M. Shu, L. M. Nadler, V. A. Boussiotis, CD28 costimulation mediates down-regulation of p27kip1 and cell cycle progression by activation of the PI3K/PKB signaling pathway in primary human T cells. *J Immunol* **168**, 2729-36 (2002).

17. A. Diz-Munoz, K. Thurley, S. Chintamen, S. J. Altschuler, L. F. Wu, D. A. Fletcher, O. D. Weiner, Membrane Tension Acts Through PLD2 and mTORC2 to Limit Actin Network Assembly During Neutrophil Migration. *PLoS Biol* **14**, e1002474 (2016).

18. A. Katsumi, J. Milanini, W. B. Kiosses, M. A. del Pozo, R. Kaunas, S. Chien, K. M. Hahn, M. A. Schwartz, Effects of cell tension on the small GTPase Rac. *J Cell Biol* **158**, 153-64 (2002).

19. T. A. Masters, B. Pontes, V. Viasnoff, Y. Li, N. C. Gauthier, Plasma membrane tension orchestrates membrane trafficking, cytoskeletal remodeling, and biochemical signaling during phagocytosis. *Proc Natl Acad Sci U S A* **110**, 11875-80 (2013).

20. A. R. Houk, A. Jilkine, C. O. Mejean, R. Boltyanskiy, E. R. Dufresne, S. B. Angenent, S. J. Altschuler, L. F. Wu, O. D. Weiner, Membrane tension maintains cell polarity by confining signals to the leading edge during neutrophil migration. *Cell* **148**, 175-88 (2012).

21. J. Rossy, J. M. Laufer, D. F. Legler, Role of Mechanotransduction and Tension in T Cell Function. *Front Immunol* **9**, 2638 (2018).

22. A. Miermont, F. Waharte, S. Hu, M. N. McClean, S. Bottani, S. Leon, P. Hersen, Severe osmotic compression triggers a slowdown of intracellular signaling, which

can be explained by molecular crowding. *Proc Natl Acad Sci U S A* **110**, 5725-30 (2013).

23. A. T. Molines, J. Lemiere, M. Gazzola, I. E. Steinmark, C. H. Edrington, C. T. Hsu, P. Real-Calderon, K. Suhling, G. Goshima, L. J. Holt, M. Thery, G. J. Brouhard, F. Chang, Physical properties of the cytoplasm modulate the rates of microtubule polymerization and depolymerization. *Dev Cell* **57**, 466-479 (2022).
24. G. Campi, R. Varma, M. L. Dustin, Actin and agonist MHC-peptide complex-dependent T cell receptor microclusters as scaffolds for signaling. *J Exp Med* **202**, 1031-6 (2005).
25. T. Wolf, W. Jin, G. Zoppi, I. A. Vogel, M. Akhmedov, C. K. E. Bleck, T. Beltraminelli, J. C. Rieckmann, N. J. Ramirez, M. Benevento, S. Notarbartolo, D. Bumann, F. Meissner, B. Grimbacher, M. Mann, A. Lanzavecchia, F. Sallusto, I. Kwee, R. Geiger, Dynamics in protein translation sustaining T cell preparedness. *Nat Immunol* **21**, 927-937 (2020).
26. B. B. Au-Yeung, J. Zikherman, J. L. Mueller, J. F. Ashouri, M. Matloubian, D. A. Cheng, Y. Chen, K. M. Shokat, A. Weiss, A sharp T-cell antigen receptor signaling threshold for T-cell proliferation. *Proc Natl Acad Sci U S A* **111**, E3679-88 (2014).
27. A. Kumar, M. Mazzanti, M. Mistrik, M. Kosar, G. V. Beznoussenko, A. A. Mironov, M. Garrè, D. Parazzoli, G. V. Shivashankar, G. Scita, J. Bartek, M. Foiani, ATR mediates a checkpoint at the nuclear envelope in response to mechanical stress. *Cell* **158**, 633-646 (2014).
28. K. Drews-Elger, M. C. Ortells, A. Rao, C. Lopez-Rodriguez, J. Aramburu, The transcription factor NFAT5 is required for cyclin expression and cell cycle progression in cells exposed to hypertonic stress. *PLoS One* **4**, e5245 (2009).

29. H. Kong, Y. Fan, J. Xie, J. Ding, L. Sha, X. Shi, X. Sun, G. Hu, AQP4 knockout impairs proliferation, migration and neuronal differentiation of adult neural stem cells. *J Cell Sci* **121**, 4029-36 (2008).

30. M. Shekarabi, R. G. Lafreniere, R. Gaudet, J. Laganiere, M. M. Marcinkiewicz, P. A. Dion, G. A. Rouleau, Comparative analysis of the expression profile of Wnk1 and Wnk1/Hsn2 splice variants in developing and adult mouse tissues. *PLoS One* **8**, e57807 (2013).

31. J. Xie, T. Wu, K. Xu, I. K. Huang, O. Cleaver, C. L. Huang, Endothelial-specific expression of WNK1 kinase is essential for angiogenesis and heart development in mice. *Am J Pathol* **175**, 1315-27 (2009).

32. S. H. Lin, I. S. Yu, S. T. Jiang, S. W. Lin, P. Chu, A. Chen, H. K. Sytwu, E. Sohara, S. Uchida, S. Sasaki, S. S. Yang, Impaired phosphorylation of Na(+)-K(+)-2Cl(-) cotransporter by oxidative stress-responsive kinase-1 deficiency manifests hypotension and Bartter-like syndrome. *Proc Natl Acad Sci U S A* **108**, 17538-43 (2011).

33. C. de Luca, T. J. Kowalski, Y. Zhang, J. K. Elmquist, C. Lee, M. W. Kilimann, T. Ludwig, S. M. Liu, S. C. Chua, Jr., Complete rescue of obesity, diabetes, and infertility in db/db mice by neuron-specific LEPR-B transgenes. *J Clin Invest* **115**, 3484-93 (2005).

34. P. Mombaerts, J. Iacomini, R. S. Johnson, K. Herrup, S. Tonegawa, V. E. Papaioannou, RAG-1-deficient mice have no mature B and T lymphocytes. *Cell* **68**, 869-877 (1992).

35. K. L. Philpott, J. L. Viney, G. Kay, S. Rastan, E. M. Gardiner, S. Chae, A. C. Hayday, M. J. Owen, Lymphoid development in mice congenitally lacking T cell receptor alpha beta-expressing cells. *Science* **256**, 1448-52 (1992).

Acknowledgments:

We thank Erik Sahai and Simon Boulton for critical reading of the manuscript. We thank Souradeep Basu, Subramanian Venkatesan, Daisy Luff, Darryl Hayward, Edina Schweighoffer, Simon Boulton, and Rob de Bruin for advice. We thank the Flow Cytometry and Biological Research Facilities of the Francis Crick Institute for flow cytometry and for animal husbandry. We thank Chou-Long Huang, Dario Alessi and Sung-Sen Yang for mouse strains.

Funding:

VLJT was supported by the Francis Crick Institute which receives its core funding from Cancer Research UK (FC001194), the UK Medical Research Council (FC001194), and the Wellcome Trust (FC001194). For the purpose of Open Access, the author has applied a CC-BY public copyright licence to any Author Accepted Manuscript version arising from this submission.

Author Contributions:

Conceptualization: JBOM, VLJT

Data curation: JBOM

Formal analysis: JBOM

Funding acquisition: VLJT

Investigation: JBOM, LV, HH, LdB, DH, RK

Methodology: JBOM, RK

Project administration: VLJT

Resources: RK

Supervision: VLJT

Visualization: JBOM

Writing – original draft: JBOM, VLJT

Writing – review & editing: JBOM, VLJT

Competing interests:

The authors have no competing interests.

Data and materials availability:

Mouse strains available on request.

List of Supplementary Materials:

Materials and Methods

Table S1

Figures S1 to S5

References 31-35

Figure 1

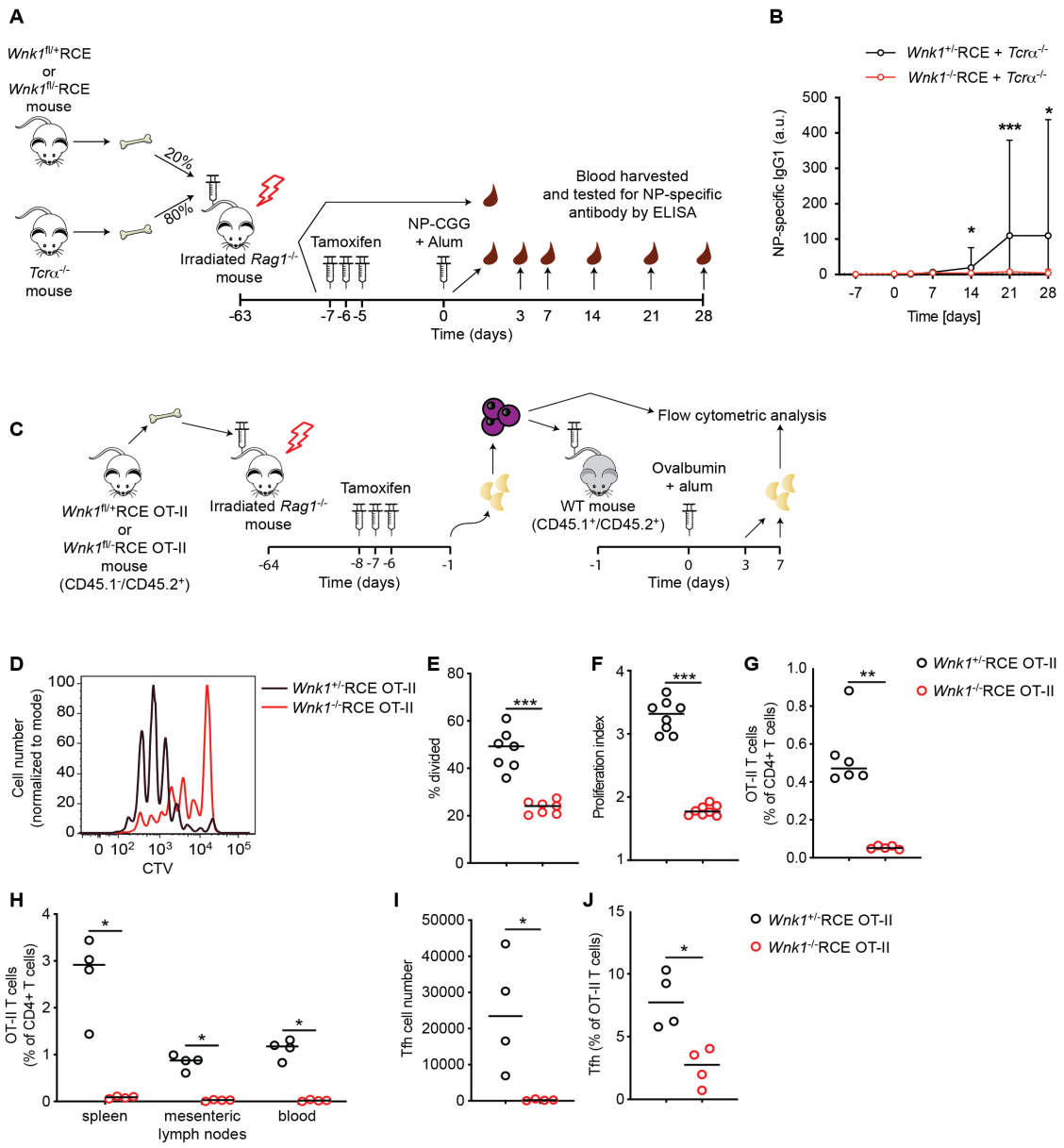

Figure 1. WNK1 is essential for the generation of T_{FH} cells and class-switched antibody responses.

(**A-B**) Irradiated RAG1-deficient mice were reconstituted with a mixture of bone marrow from TCRα-deficient (TCRα$^{-/-}$) mice and either *Wnk1*$^{fl/+}$RCE or *Wnk1*$^{fl/-}$RCE mice, treated with tamoxifen at least 8 weeks later to delete *Wnk1*^{fl} alleles and immunized with NP-CGG in alum (A). Median (± 95% CI) NP-specific IgG1 antibodies in the serum quantified by

ELISA at the time points indicated (B) (n = 10-18). (**C-J**) Irradiated RAG1-deficient mice were reconstituted with bone marrow from *Wnk1*$^{fl/+}$RCE OT-II or *Wnk1*$^{fl/-}$RCE OT-II mice, treated with tamoxifen, and 7 d later naïve *Wnk1*$^{+/-}$ or *Wnk1*$^{-/-}$ CD4^{+} OT-II T cells (CD45.1^{-} CD45.2^{+}) were isolated, labelled with CTV, adoptively transferred into WT (CD45.1^{+}CD45.2^{+}) mice that were subsequently immunized with OVA in alum, and 3 or 7 days later, lymph node cells were analyzed by flow cytometry (C). CTV dilution at day 3 (D) was used to calculate the percentage of cells that had divided at least once (E, n = 7) and the proliferation index (average number of divisions by dividing cells) (F, n = 8). CD4^{+}CD45.1^{-}CD45.2^{+} OT-II T cells as a percentage of all CD4^{+} cells in peripheral and mesenteric lymph nodes at day 3 (G), and in the indicated tissues at day 7 (H, n=4). Splenic T_{FH} (PD-1^{hi}CXCR5^{+}) cell numbers (I) and percentage of all OT-II T cells day 7 (J, n=4). Each point represents a different mouse. Horizontal lines show median. Data are from 1 experiment representative of 2 (G) or 3 (H-J) experiments, or pooled from 2 independent experiments (B, E-F). a.u., arbitrary units. Statistical analysis with the Mann-Whitney U test. *$0.01 < p < 0.05$; **$0.001 < p < 0.01$; ***$0.0001 < p < 0.001$.

Figure 2

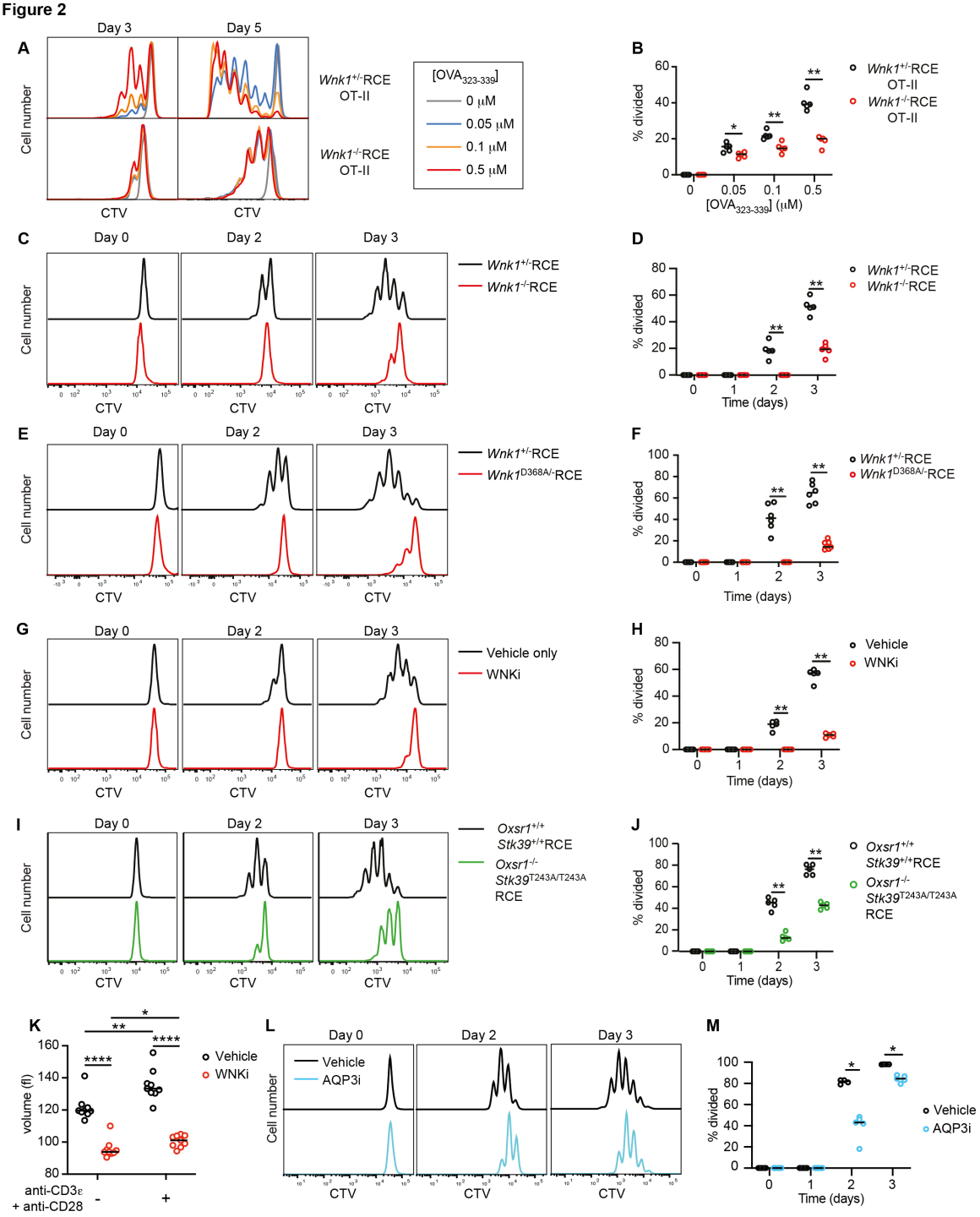

Figure 2. WNK1, OXSR1, STK39 and AQP3 are required for TCR-induced proliferation of CD4⁺ T cells.

(**A-B**) WNK1-expressing or -deficient CTV-labelled OT-II CD4⁺ T cells were co-cultured with bone marrow-derived APCs in the presence of indicated concentrations of $OVA_{323-339}$

peptide for 5 days. CTV dilution (A) was used to determine the percentage of cells that had divided at day 3 (n = 5) (B). (**C**-**J**, **L-M**) Naïve $CD4^+$ CTV-labelled T cells of the indicated genotypes (C-F, I-J) or treated with WNKi (G-H) or AQP3i (L-M) were activated on plate-bound anti-CD3ε and anti-CD28 antibodies for indicated times. CTV dilution (C, E, G, I, L) was used to determine the percentage of cells that had divided (n = 4-7) (D, F, H, J, M). (**K**) Mode volume of naïve WT $CD4^+$ T cells cultured for 1 h in the presence of vehicle only or WNKi on plate-bound anti-CD3ε and anti-CD28 antibodies where indicated (n = 9). Each point represents a different mouse; horizontal lines show median; data are from 1 experiment representative of 2 (B, H, M) or 3 (D, J) experiments, or pooled from 2 independent experiments (F, K). Statistical analysis with the Mann-Whitney U test. *$0.01 < p < 0.05$; **$0.001 < p < 0.01$.

Figure 3

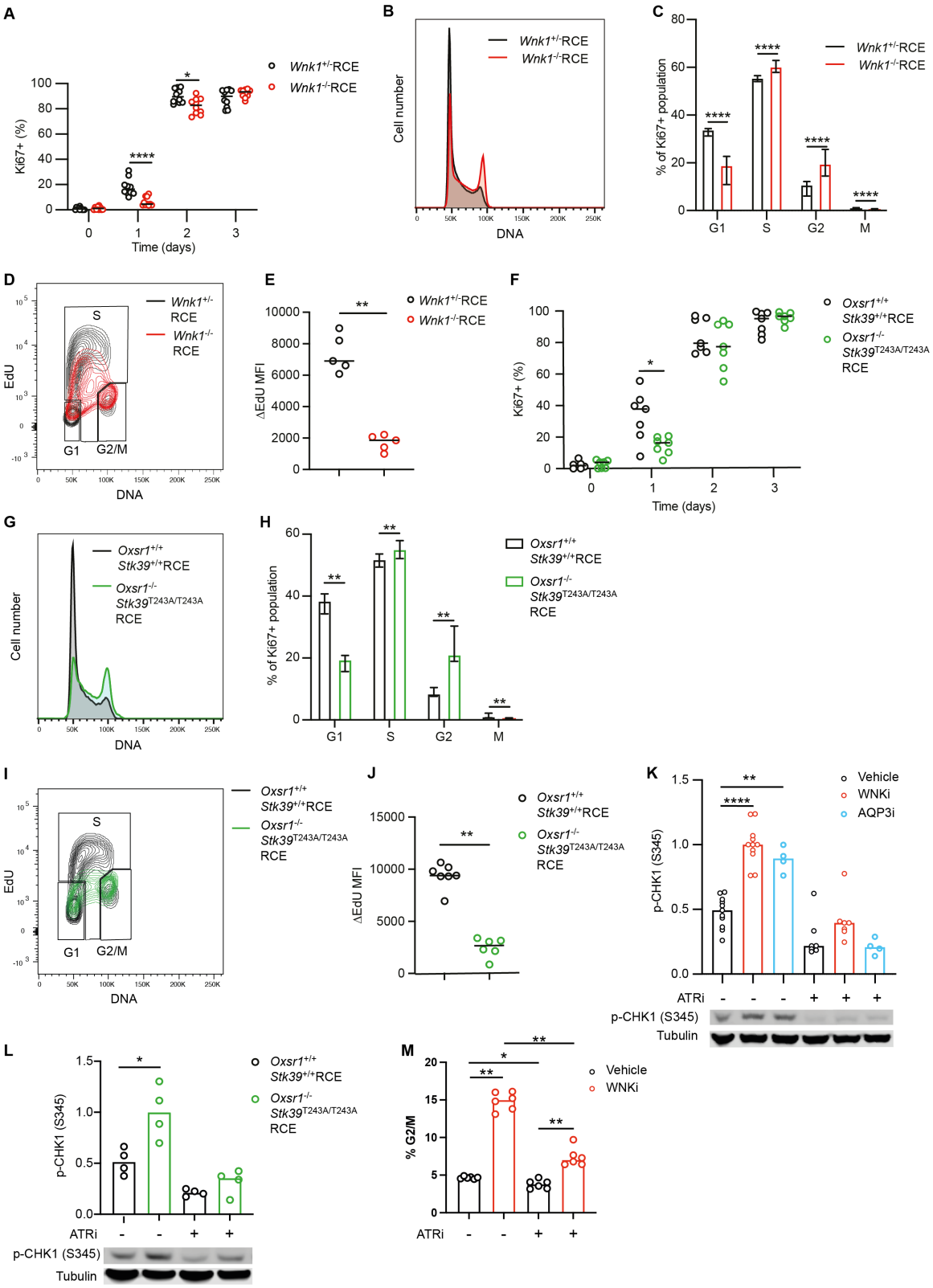

Figure 3. Loss of WNK1, OXSR1, STK39 or AQP3 impairs cell cycle progression of

CD4$^+$ T cells and activates the ATR-mediated G2/M checkpoint.

(**A-J**) Naive CD4$^+$ T cells of the indicated genotypes, or treated with indicated inhibitors, were activated on plate-bound anti-CD3ε and anti-CD28 antibodies for 3 days. Graphs show percentage of Ki67$^+$ cells (after adjusting for population expansion) (A, F), and DNA content of Ki67$^+$ cells (B, G) which was used to estimate the median (± 95% CI) percentage of cells in different cell cycle phases (C, H). Cells were pulsed with EdU for 10 min and incorporation of EdU (D, I) was used to calculate the rate of EdU incorporation (ΔEdU) by subtracting the average EdU MFI in G1 and G2/M phase cells from the average EdU MFI in S phase (n = 5-7) (E, J) using the gates shown. (**K-M**) CD4$^+$ T cells were cultured for 3 d on plate-bound anti-CD3ε and anti-CD28 antibodies, with ATRi or vehicle only added to cultures for the final 36 h. Graph of the abundance of p-CHK1 (S345) determined using immunoblots (example immunoblots below graph) (K, L) (n = 4-11). p-CHK1 was normalized to tubulin and to the mean signal in WNKi-treated cells (K) or *Oxsr1*$^{-/-}$ *Stk39*$^{T243A/T243A}$RCE cells (L) which was set to 1. Graph showing percentage of CD4$^+$ cells in G2/M phase (EdU$^-$, 4n), gating as in Fig. S4E (n = 6) (M). Each point represents a different mouse; horizontal lines or columns show median; data pooled from 2 independent experiments (A, C, F, H, J, L, M) or from 1 experiment representative of 2 (E) or 5 (K) experiments. Statistical analysis with the Mann-Whitney U test. * $0.01 < p < 0.05$; ** $0.001 < p < 0.01$. *** $0.0001 < p < 0.001$. **** $p < 0.0001$.

Figure 4

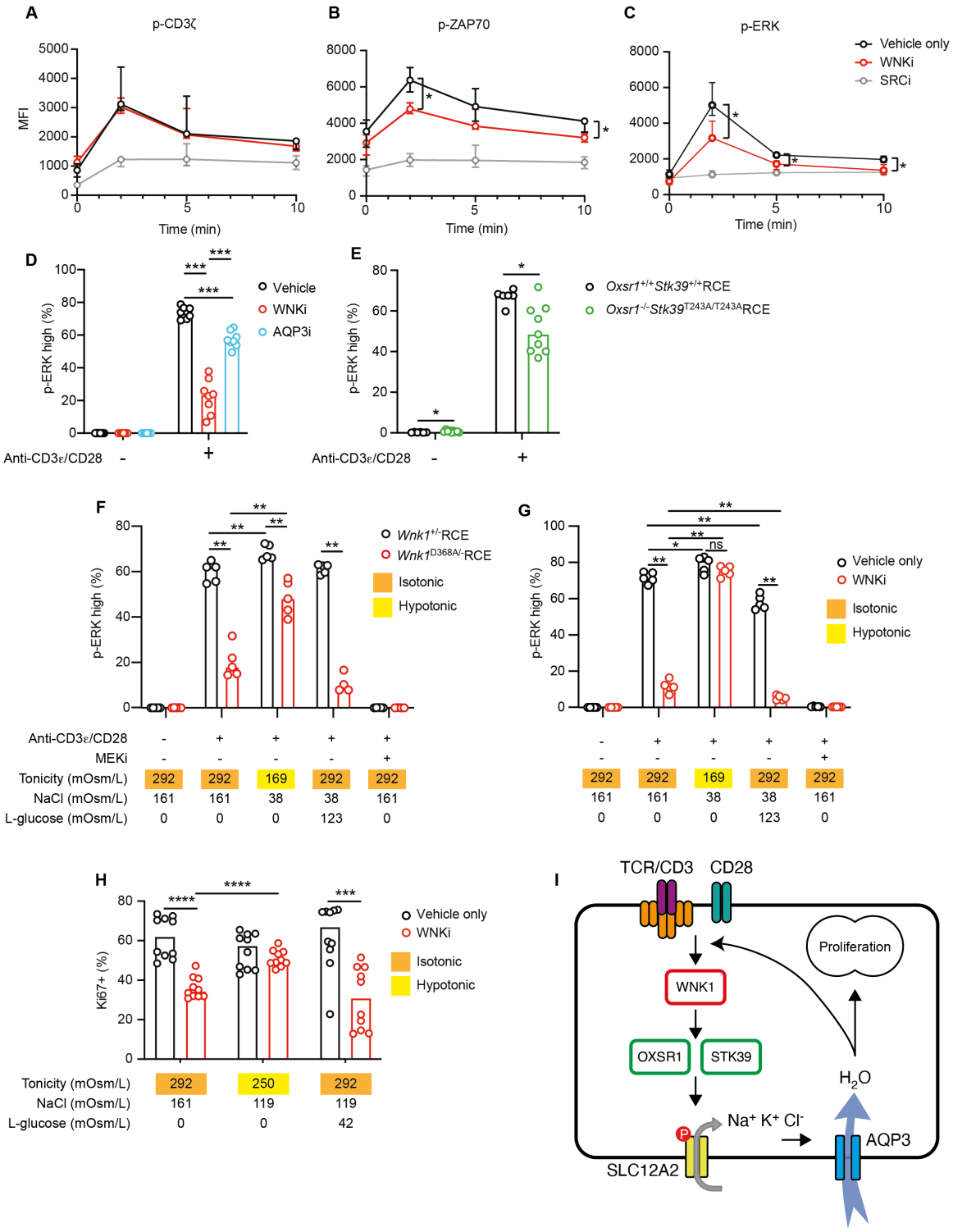

Figure 4. WNK1-dependent water influx is required for TCR signaling and G1 entry.

(**A**-**C**) Naïve WT $CD4^+$ T cells were activated using soluble anti-CD3ε and anti-CD28 antibodies in the presence of indicated inhibitors and analyzed by flow cytometry. Graphs show median (± 95% CI) levels of p-CD3ζ (Y142) (A), p-ZAP70 (Y319) (B), and p-ERK1/2 (T202/Y204) (C) (n = 4). (**D-G**) $CD4^+$ T cells were cultured for 1 h in the presence or absence of plate-bound anti-CD3ε and anti-CD28 antibodies and indicated inhibitors. In some cultures, tonicities were altered by modulating concentrations of NaCl and L-glucose (F, G). Graphs show the percentage of cells that were p-ERK high as determined by flow cytometry, gating as in Fig. S5A (n = 5-9). (**H**) $CD4^+$ T cells were cultured on plate-bound anti-CD3ε and anti-CD28 antibodies for 2 days at the indicated tonicities. Graph shows percentage of $Ki67^+$ cells (after adjusting for population expansion) measured by flow cytometry (n = 10). (**I**) Proposed model of how TCR/CD28 signals via WNK1, OXSR1, STK39 and SLC12A-family ion co-transporters (SLC12A2 shown) lead to ion influx and subsequent water entry through AQP3 by osmosis, which is required for TCR/CD28 signaling and T cell proliferation. Each point represents a different mouse; columns show median. Data pooled from 2 (A-D, H) or 3 (E) independent experiments or from 1 experiment representative of >2 (F,G) experiments. Statistical analysis carried out using the Mann-Whitney U test. ns, not significant; * $0.01 < p < 0.05$; ** $0.001 < p < 0.01$. *** $0.0001 < p < 0.001$. **** $p < 0.0001$.

SUPPLEMENTARY MATERIAL

MATERIALS AND METHODS

Mice

Mice with a conditional allele of *Wnk1* containing loxP sites flanking exon 2 (*Wnk1*^{tm1Clhu},*Wnk1*^{fl}) (*31*), with a deletion of exon 2 of *Wnk1* (*Wnk1*$^{tm1.1Clhu}$, *Wnk1*$^{-}$), with a kinase-inactive allele of *Wnk1* (*Wnk1*$^{tm1.1Tyb}$, *Wnk1*^{D368A}) (*9*), with a conditional allele of *Oxsr1* containing loxP sites flanking exons 9 and 10 (*Oxsr1*$^{tm1.1Ssy}$, *Oxsr1*^{fl}) (*32*), with a tamoxifen-inducible Cre in the ROSA26 locus (*Gt(ROSA)26Sor*$^{tm1(Cre/ESR1)Thl}$, *ROSA26*^{CreERT2}, RCE) (*33*), with an allele of *Stk39* encoding STK39-T243A (*Stk39*$^{tm1.1Arte}$, *Stk39*^{T243A}) (*12*) that cannot be activated by WNK1, deficient for RAG1 (*Rag1*^{tm1Mom}, *Rag1*$^{-}$) (*34*) or TCRα (*Tcra*^{tm1Mjo}, *Tcrα*$^{-}$) (*35*), and with transgenes encoding TCRα and TCRβ chains specific for chicken ovalbumin residues 323-339 (Tg($^{TcraTcrb)425Cbn}$,OT-II) (*10*) have been described before. C57BL/6J and B6SJLF1 mice were provided by the Biological Research Facility of the Francis Crick Institute. All genetically modified mice were maintained on a C57BL/6J background, housed in specific pathogen-free conditions, and given food and water *ad libitum*. All experiments were approved by the Francis Crick Institute Animal Welfare Ethical Review Board and were carried out under the authority of a Project Licence granted by the UK Home Office.

Bone marrow chimeras

RAG1-deficient recipient mice were irradiated with 1 dose of 5 Gy from a ^{37}Cs source. Bone marrow cells were transferred intravenously into irradiated recipient mice which were maintained on 0.02% enrofloxacin (Baytril, Bayer Healthcare) for 4 weeks. Both male and female mice were used, but in all cases the sex of the donor and recipient mice was matched. The hematopoietic compartment was allowed to reconstitute for at least 8 weeks

after bone marrow transfer. In all experiments, control and experimental chimeric mice or cells derived from them were always age- and sex-matched.

In vivo deletion of floxed alleles

Mice were injected intraperitoneally with 2 mg tamoxifen (Sigma-Aldrich) in 100μL of corn oil (Sigma-Aldrich) on 3 (*Wnk1*^{fl}) or 5 (*Oxsr1*^{fl}) consecutive days. Mice were sacrificed 7 (*Wnk1*^{fl}) or 21 (*Oxsr1*^{fl}) days after initial tamoxifen injection.

NP-CGG immunization and ELISA

Mice were injected intraperitoneally with 50μg of 4-hydroxy-3-nitrophenylacetyl (NP)-CGG (BioSearch Technologies) in PBS, 25% Alum (Thermo Fisher Scientific). Blood was collected from the lateral tail vein at the indicated time points, allowed to clot, then centrifuged at 17,000 x *g* for 10 min. NP_{20}-BSA (bovine serum albumin) (5μg/ml, Santa Cruz Biotechnology) was used to coat 96-well Maxisorp Immunoplates (Nalge Nunc International Corporation) overnight at 4°C. Plates were washed with PBS, 0.01% Tween-20 (PBS-T), blocked with 3% BSA in PBS, and washed with PBS, 0.01% Tween-20. Serial dilutions of sera were incubated on the NP_{20}-BSA-coated plates overnight at 4°C. Plates were washed 3 times with PBS-T and incubated with 1.6 μg/ml biotin-conjugated goat anti-mouse IgM (Thermo Fisher Scientific) or 4 μg/ml biotin-conjugated goat anti-mouse IgG1 (Thermo Fisher Scientific) for 2 h at room temperature. Plates were washed with PBS-T 3 times, incubated with 1 μg/ml peroxidase-labelled streptavidin (Vector laboratories) for 2 h at room temperature, washed 5 times with PBS-T and incubated with 1x TMB ELISA substrate solution (Thermo Fisher Scientific). The reaction was stopped with 2 N H_2SO_4. Absorption at 450 nm was measured using the SpectraMax 190 (Molecular Devices LLC.). Serum concentrations of NP-specific IgG and IgM antibodies were calculated in arbitrary

units (a.u.) from the linear section of the response curves.

Cell isolation

Blood was harvested from live mice by cutting the lateral tail vein. Peripheral lymph nodes, mesenteric lymph nodes and spleens were dissociated into single cell suspensions by mashing through a 70 μm filter. Bone marrow from the hind limbs was harvested by flushing femurs and tibias with media. Blood, bone marrow, and spleen samples were treated with ACK buffer (155 mM NH_4Cl, 10 mM $KHCO_3$, 0.1 mM Na_2EDTA) for 3 min at room temperature to remove erythrocytes, washed and resuspended in PBS. ACK treatment was repeated twice for blood samples. To isolate naive $CD4^+$ T cells, lymph node cells were resuspended in a mixture of biotinylated antibodies against CD8, CD11b, CD11c, B220, CD19, CD25, CD44, and GR-1 (Table S1) in IMDM (35.93 mM NaCl, 0.18 mM Penicillin, 0.17 mM Streptomycin, IMDM powder, pH 7.2 [Thermo Fisher Scientific]), 5% fetal calf serum (FCS) for 20 min at 4°C. Cells were incubated with streptavidin-coated Dynabeads (Thermo Fisher Scientific) in IMDM, 5% FCS for 20 min at 4°C. Cell and bead suspensions were placed on a magnet for 2 min at room temperature and the bead-depleted fraction was collected.

CTV labelling of $CD4^+$ T cells

Naïve CD4+ T cells were incubated in PBS with CellTrace Violet (CTV, ThermoFisher) at a concentration of 5 μM (for OT-II T cells) or 2.5 μM (for polyclonal T cells) for 10 min at 37°C. A 5-fold excess of pre-warmed RPMI+ medium (RPMI-1640, 100 μM non-essential amino acids, 20 mM HEPES [Thermo Fisher Scientific], 10% FCS, 100 U/mL Penicillin, 100 μg/mL Streptomycin, 2 mM L-glutamine, 100 μM 2-mercaptoethanol [Sigma-Aldrich]) was added to the cells for a further 7 min. Cells were then pelleted and resuspended in

the appropriate media.

RNA isolation and quantitative reverse transcription- quantitative polymerase chain reaction (RT-qPCR)

RNA was purified from at least 5 x 10^4 $CD4^+$ T cells using the RNeasy Micro kit (Qiagen). cDNA was synthesized using the SuperScript™VILO™cDNA synthesis kit (Invitrogen). Taqman™ Gene Expression Assays (Thermo Fisher Scientific) were used to measure *Wnk1* (exon boundary 1-2, Mm01184006_m1), and *Hprt* (exon boundary 2-3, Mm03024075_m1). Fluorescence was measured using a QuantStudio 3 or QuantStudio 5 qPCR machine (Thermo Fisher Scientific).

Adoptive transfer of OT-II $CD4^+$ T cells

OT-II T cells ($CD45.1^-CD45.2^+$) were isolated from peripheral and mesenteric lymph nodes, labeled with CTV and 1 x 10^6 (for day 3 analysis) or 35 x 10^3 (for day 7 analysis) OT-II T cells were injected into the tail vein of B6SJLF1 mice ($CD45.1^+CD45.2^+$). 24 h later (day 0) mice were immunized with 50 μg (day 3 analysis) or 100 μg (day 7 analysis) chicken ovalbumin (OVA) protein (InvivoGen) in PBS, 25% Alum (Thermo Fisher Scientific) by intraperitoneal injection. Peripheral and mesenteric lymph nodes were harvested at day 3. Mesenteric lymph nodes, spleen and blood were harvested at day 7.

Co-culture of OT-II T cells with APCs

To generate APCs, bone marrow from C57BL/6J mice was treated with ACK and cultured in DC medium (RPMI-1640 [Thermo Fisher Scientific], 10% FCS, 100 U/mL Penicillin, 100 μg/mL Streptomycin, 2 mM L-glutamine [Sigma-Aldrich]) with GM-CSF (20 ng/ml, Peprotech) at 10^6 cells/ml for 10 d at 37°C. GM-CSF was replenished at days 3, 5 and 7.

Naïve $CD4^+$ OT-II T cells and APCs (both at 2.5 x 10^5 cells/ml) were co-cultured in round-bottomed 96-well plates in DC medium (RPMI-1640, 10% FCS, 100 U/mL Penicillin, 100 μg/mL Streptomycin, 2 mM L-glutamine [Sigma-Aldrich]) the presence of indicated concentrations of $OVA_{323-339}$ peptide (Sigma) for the indicated times.

Activation of T cells with plate-bound anti-CD3ε and anti-CD28 antibodies

Flat-bottomed multi-well cell culture plates (Corning) were incubated overnight at 4°C with PBS containing anti-CD3ε and anti-CD28 antibodies (4 μg/ml). Naïve $CD4^+$ T cells from peripheral and mesenteric lymph nodes were cultured at 1x10^6 cells/ml in RPMI+ at 37°C. Where indicated, cells were activated in the presence of 2.5 μM WNKi (WNK463, MedChem Express) or 20 μM AQP3i (DFP00173, Axon MedChem) which were added from a stock solution in DMSO or the equivalent amount of DMSO as a vehicle only control. 1 μM ATRi (AZD6738, Selleckchem) or 4 mM hydroxyurea (HU, Sigma-Aldrich) were added for the final 36 h or 2 h of culture, respectively. For 1 h stimulations, naïve T cells were treated with 2.5 μM WNKi, 1μM MEKi (PD0325901, Selleckchem), or vehicle only and transferred into anti-CD3ε/anti-CD28-coated multi-well plates, centrifuged at 340 x *g* for 30 s and incubated at 37°C for 1 h, still in the presence of inhibitors. To culture cells at different osmolarities, the concentration of NaCl in RPMI+ medium was adjusted and the osmolarity verified using an osmometer (Model 3250, Thermo Fisher Scientific). In some cases, isotonic (292 mOsm/l) RPMI+ medium was used in which some NaCl was replaced with L-glucose, an inert osmolyte.

Activation of T cells with soluble anti-CD3ε and anti-CD28 antibodies

Naïve $CD4^+$ T cells were incubated in IMDM (Thermo Fisher Scientific), 0.5% FCS for 1 h at 37°C, cooled at 4°C for 10 min and then incubated with anti-CD3ε and anti-CD28

antibodies (10 μg/ml) in RPMI, 0.5% FCS in the presence of 2.5 μM WNKi, 100 nM SRCi (Dasatinib, Sigma-Aldrich) or vehicle only at 4°C for 30 min. Unstimulated (0 min) samples were incubated in the presence of relevant inhibitors but without anti-CD3ε or anti-CD28 antibodies. Cells were warmed to 37°C for 15 min and then stimulated with the addition of 80 μg/mL anti-Armenian hamster IgG (Antibodies-online.com). Activation was stopped at the indicated time point with the addition of 2% paraformaldehyde (PFA).

Cell volume measurements

Naïve $CD4^+$ T cells were rested overnight in RPMI+ with 1 mM pyruvate. Samples were enriched for live cells by incubating in PBS at 37°C for 10 min followed by 7 min at 37°C in RPMI+ with 1 mM pyruvate. Cells were then treated with vehicle only or 2.5 μM WNKi and placed in cell culture plates ± plate-bound anti-CD3ε and anti-CD28 for 1 h at 37°C. Cell volume was measured using the CASY cell counter (OMNI Life Science).

Flow cytometry

Proliferation analysis

Cells were stained in PBS containing fluorophore-conjugated antibodies (Table S1) and LIVE/DEAD™ Near-IR dye (Thermo Fisher Scientific) (1:500) at 4°C for 20 min, and resuspended in FACS buffer (PBS, 0.5% BSA). For cell counting, a known number of Calibrate APC beads (BD biosciences) were added to the sample. Samples were analyzed on an LSRFortessa™ (BD biosciences) flow cytometer. Flow cytometry data were analyzed using FlowJo 9 and 10 (BD Biosciences).

CXCR5

Cells were incubated in PBS, 2% FCS containing biotinylated anti-CXCR5 antibody at

37°C for 30 min. Cells were washed, incubated with fluorophore-conjugated streptavidin for 15 min at room temperature, washed, resuspended in FACS buffer, and analyzed on the flow cytometer.

Analysis of phosphorylated proteins

Cells were fixed in 2% PFA at 4°C for 15 min, permeabilized with 90% methanol overnight at -20°C, washed 3 times and then incubated with the relevant primary antibody (Table S1) in PBS, 2% FCS for 30 min at room temperature. Cells were then washed, stained with the relevant secondary antibody in PBS, 2% FCS for 30 min at room temperature, washed, resuspended in FACS buffer, and analyzed on the flow cytometer.

Cell cycle analysis

To analyze the rate of S phase progression, 10 μM EdU (5-ethynyl-2'-deoxyuridine, Jena Bioscience) was added to the cell culture medium for 10 min at the end of 72 h culture on anti-CD3ε- and anti-CD28-coated cell culture plates. Cells were fixed in 4% PFA, permeabilized in BD Perm/Wash™ buffer (BD biosciences), 1% BSA at room temperature for 15 min. The Click reaction was initiated by adding 2 mM $CuSO_4$, 0.3125 μM AF488-azide, 10 mM Sodium Ascorbate (all from Jena Bioscience) in TBS (50 mM Tris, 150 mM NaCl, pH 7.5) for 30 min at room temperature. To analyze distribution of cells in different phases of the cell cycle, cells were stained with Live/Dead-Near IR stain (ThermoFisher Scientific) and fixed in 4% PFA for 15 min at 4°C, stained with fluorophore-conjugated antibodies against Ki67, p-MPM2 (Table S1) in BD Perm/Wash™ buffer (BD biosciences) containing 2% FCS for 30 min at room temperature, resuspended in BD Perm/Wash™ buffer containing 1 μg/mL FxCycle™ Violet (Thermo Fisher Scientific) to stain for DNA content, incubated at room temperature for 30 min, and analyzed on the flow cytometer.

In some experiments, cells were pulsed with EdU and analyzed as above. Ki67 was used to identify cells that had exited G0. The proportion of cells in G1, S, and G2/M was estimated using the Watson model generated from the histogram of DNA content of $Ki67^+$ cells. Staining for p-MPM2 was used to identify cells in M phase. Where indicated, cells were pulsed for 30 min with EdU at the end of 72 h culture and G2/M cells were identified as the 4n EdU^- population. The effect of expansion was taken out of the data by dividing the total number of $Ki67^+$ cells by the expansion index - the fold expansion of the population due to proliferation estimated by generating a model using CTV dilution histograms – to give $Ki67^+_{adjust}$. The percentage of $Ki67^+$ cells in the population if no division had taken place was then calculated as follows: $(Ki67^+_{adjust})/(Ki67^+_{adjust} + Ki67^-) \times 100\%$.

Immunoblot analysis

Cell pellets were thawed at room temperature, lysed using RIPA buffer (50 mM Tris, 150 mM NaCl, 50 mM NaF, 2 mM EDTA, 2 mM $Na_4P_2O_7$, 1 mM Na_3VO4, 1% Triton X-100, 0.5% deoxycholate, 0.1% SDS, 1 mM PMSF, cOmplete™ EDTA-free protease inhibitor cocktail [Roche], PhosSTOP™ [Roche]), centrifuged at 17,000 x *g* for 15 min at 4°C and the supernatant was collected. The protein concentration of each sample was determined using the Pierce™ BCA protein assay kit (Thermo Fisher Scientific) according to the manufacturer's instructions. Samples were mixed with NuPage™ LDS sample buffer (Thermo Fisher Scientific), 50 mM DTT and loaded onto NuPAGE™ 4-12% Bis-Tris precast polyacrylamide gels (Thermo Fisher Scientific) with the volume of each sample adjusted to ensure equal protein amounts per well. Electrophoresis was carried out at 200 V for 53 min in NuPAGE™ MOPS or MES SDS running buffer (Thermo Fisher Scientific). Proteins were transferred to a methanol-activated polyvinylidene difluoride membrane in NuPAGE™ transfer buffer (Thermo Fisher Scientific) at 30 V for 65 min. Membranes were blocked with Odyssey® blocking buffer (LI-COR) for 1 h at room temperature, incubated

with primary antibody (Table S1) in Odyssey® blocking buffer overnight at 4 °C, washed 3 times with TBS-T (TBS, 0.05% Tween20), incubated with fluorophore-conjugated secondary antibody (Table S1) in Odyssey® blocking buffer for 1 h at room temperature, washed 3 times with TBS-T, and imaged using the Odyssey® CLx (LI-COR). Image Studio Lite (LI-COR) was used to quantify intensities of bands.

Statistical analysis

The non-parametric Mann-Whitney U-test was used to analyze the difference between groups using GraphPad Prism 8.

Table S1. Antibodies used in this study.

Antigen	Clone	Supplier	Dilution
ERK	3A7	Cell Signaling Technology	1:1000 (Immunoblot)
OXSR1	Polyclonal	MRC PPU Reagents and services	1:1000 (Immunoblot)
p-CHK1 (S345)	133D3	Cell Signaling Technology	1:1000 (Immunoblot)
p-OXSR1 (S325)	Polyclonal	MRC PPU Reagents and Services	1:1000 (Immunoblot)
p-RPA32 (S4/8)	Polyclonal (#A300-245A)	Bethyl Laboratories	1:1000 (Immunoblot)
α-Tubulin	TAT-1	Cell Services STP, Crick	1:15000 (Immunoblot)
γH2AX (S139)	JBW301	Merck Millipore	1:10000 (Immunoblot)
Mouse IgG	IRDye® 800CW	LI-COR Biosciences	1:4000 (Immunoblot)
Mouse IgG	Alexa Fluor 680	ThermoFisher Scientific	1:4000 (Immunoblot)
Rabbit IgG	IRDye® 800CW	LI-COR Biosciences	1:4000 (Immunoblot)
Rabbit IgG	Alexa Fluor 680	ThermoFisher	1:4000

		Scientific	(Immunoblot)
Sheep IgG	Alexa Fluor 680	ThermoFisher Scientific	1:4000 (Immunoblot)
CD3ε	145-2C11	Tonbo Biosciences	1:125 (plate-bound stimulation) 1:50 (soluble stimulation)
CD28	37.51	Biolegend	1:250 (plate-bound stimulation) 1:100 (soluble stimulation)
Hamster IgG (H&L chain)	Polyclonal (#ABIN101378)	Antibodies-online.com	1:25 (soluble stimulation)
CD4	GK1.5	ThermoFisher Scientific	1:200 (FACS)
CD45.1	A20	ThermoFisher Scientific	1:100 (FACS)
CD45.2	104	Biolegend	1:100 (FACS)
CXCR5	2G8	BD Biosciences	1:100 (FACS)
Ki67	SolA15	ThermoFisher Scientific	1:100 (FACS)
p-CD3ξ (Y142)	K25-407.69	BD Biosciences	1:400 (1.25□g/mL) (FACS)
p-ERK1 (T202/Y204)	Polyclonal (#9101)	Cell Signaling Technology	1:50 (FACS)

p-ERK2 (T185/Y187)	Polyclonal (#9101)	Cell Signaling Technology	1:50 (FACS)
p-MPM2 (S/TP motif)	MPM-2	Merck Millipore	1:100 (FACS)
p-ZAP-70 (Y319)	65E4	Cell Signaling Technology	1:400 (FACS)
PD-1	29F.1A12	Biolegend	1:100 (FACS)
Mouse IgG (H&L chain)	Donkey polyclonal (highly cross-adsorbed) – AF488	ThermoFisher Scientific	1:500 (FACS)
Rabbit IgG (H&L chain)	Goat polyclonal (highly cross-adsorbed) – AF647	ThermoFisher Scientific	1:500 (FACS)
Streptavidin	APC	ThermoFisher Scientific	1:500 (FACS)

Supplementary Figures

Figure S1

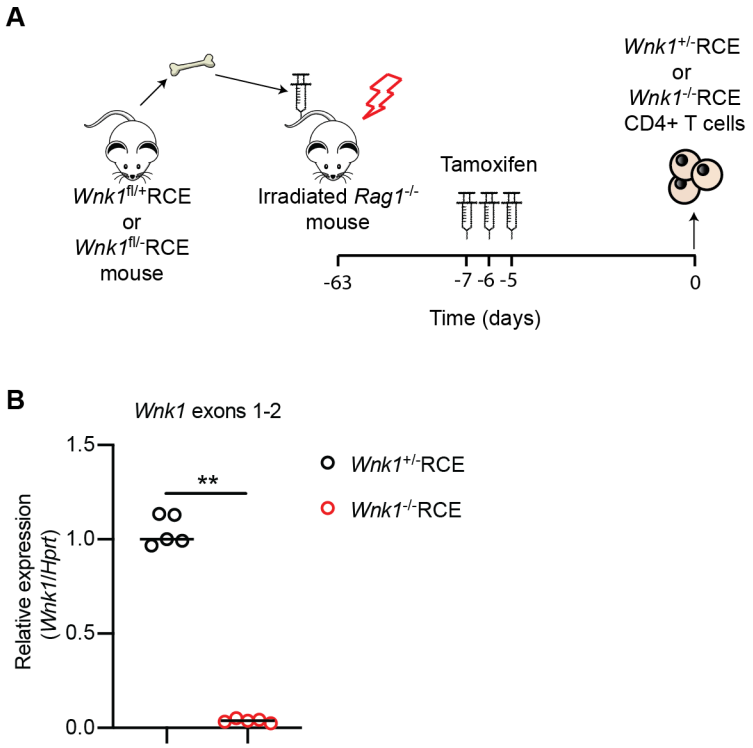

Figure S1. Generation of WNK1-deficient T cells.

(**A**) Bone marrow from *Wnk1*$^{fl/+}$/RCE and *Wnk1*$^{fl/-}$/RCE mice was transferred into irradiated RAG1-deficient mice. At least 8 weeks later, the chimeras were treated with tamoxifen on three successive days. Lymph nodes were harvested 7 d after start of tamoxifen treatment and WNK1-expressing (*Wnk1*$^{+/-}$RCE) or WNK1-deficient (*Wnk1*$^{-/-}$RCE) naive CD4^{+} T cells purified. (**B**) Graph of qPCR measurement of mRNA levels of *Wnk1* (exons 1-2) relative to *Hprt* in *Wnk1*$^{+/-}$RCE and *Wnk1*$^{-/-}$RCE naïve CD4^{+} T cells generated as in A, normalized to median level in *Wnk1*$^{+/-}$RCE T cells which was set to 1 (n = 5). Each point represents a different mouse; horizontal lines show median; data pooled from 2 independent experiments. Statistical analysis carried out using the Mann-Whitney U test. ** $0.001 < p < 0.01$.

Figure S2

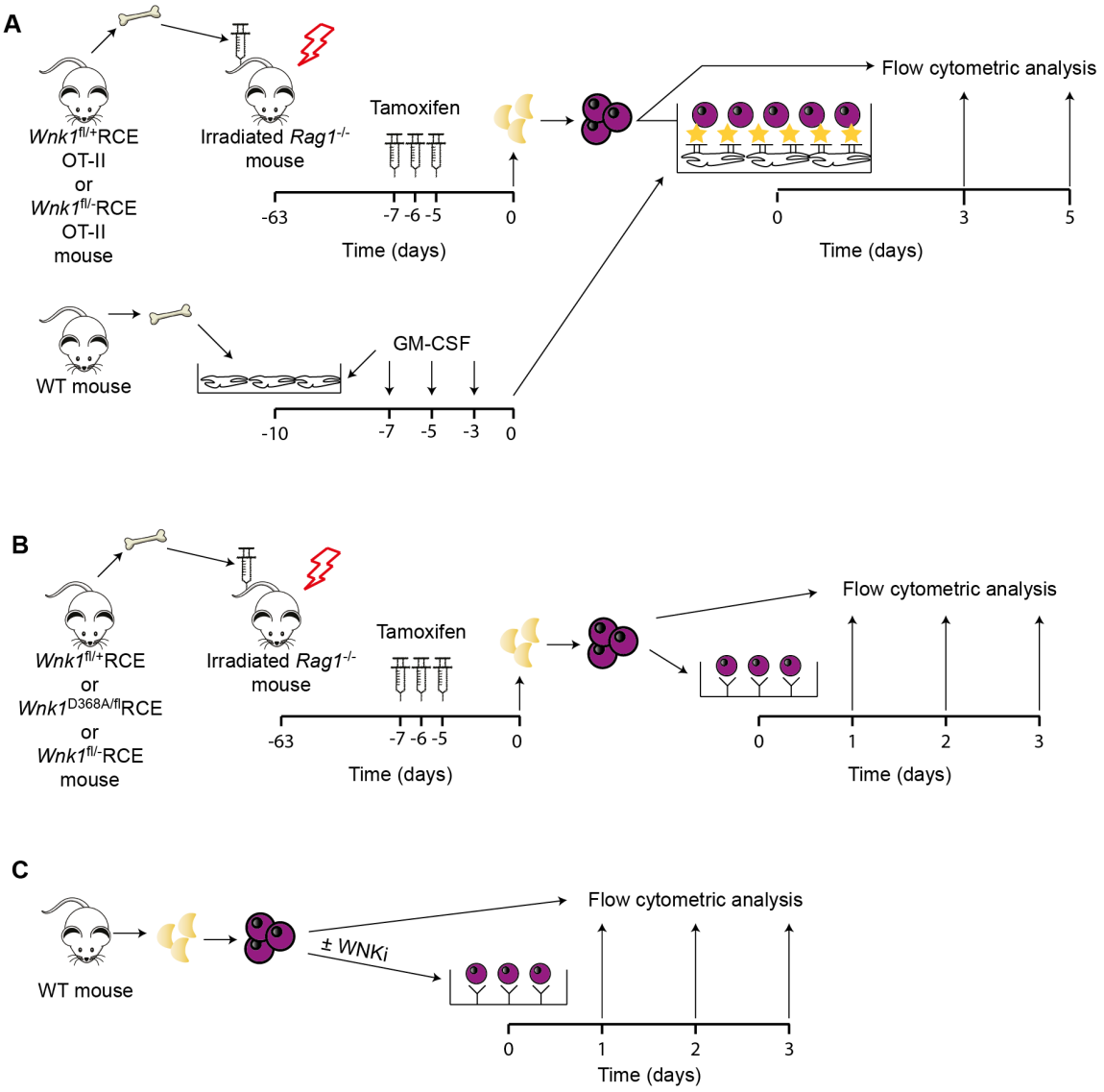

Figure S2. *In vitro* analysis of activation of WNK1-deficient CD4⁺ T cells.

(**A**) Bone marrow from *Wnk1*$^{fl/+}$RCE OT-II and *Wnk1*$^{fl/-}$RCE OT-II mice was transferred into irradiated RAG1-deficient mice. At least 8 weeks later, the chimeras were treated with tamoxifen on three successive days to delete the floxed exon 2 of *Wnk1*, lymph nodes harvested 7 d after start of tamoxifen treatment and WNK1-expressing (*Wnk1*$^{+/-}$RCE OT-II) or WNK1-deficient (*Wnk1*$^{-/-}$RCE OT-II) naive CD4^{+} T cells purified. APCs were generated from WT bone marrow cells cultured in GM-CSF containing medium for 10 d.

T cells were labelled with CTV and co-cultured with APCs for up to 5 days, in the presence of indicated concentrations of $OVA_{323-339}$ peptide and analyzed by flow cytometry. (**B**) Bone marrow from *Wnk1*$^{fl/+}$RCE, *Wnk1*$^{fl/-}$RCE or *Wnk1*$^{D368A/fl}$RCE mice was transferred into irradiated RAG1-deficient mice. At least 8 weeks later, the chimeras were treated with tamoxifen on three successive days, lymph nodes harvested 7 d after start of tamoxifen treatment and WNK1-expressing (*Wnk1*$^{+/-}$RCE), WNK1-deficient (*Wnk1*$^{-/-}$RCE) or WNK1-D368A expressing (*Wnk1*$^{D368A/-}$RCE) naive $CD4^+$ T cells were purified. T cells were labelled with CTV and activated using plate-bound anti-CD3ε and anti-CD28 antibodies and analyzed by flow cytometry up to 3 d later. (**C**) WT naïve $CD4^+$ T cells were labelled with CTV, activated on anti-CD3ε and anti-CD28 antibodies in the presence or absence of WNKi and analyzed at indicated time points.

Figure S3

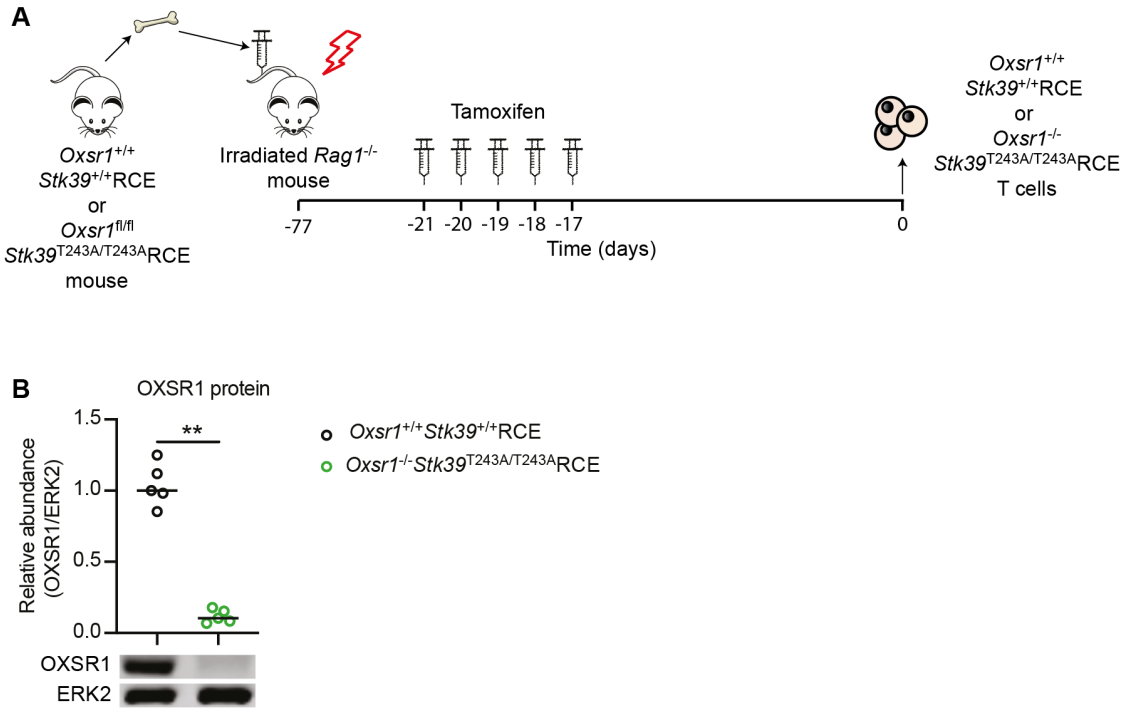

Figure S3. Generation of CD4$^+$ T cells with mutations in both *Oxsr1* and *Stk39*.

(**A**) Bone marrow from *Oxsr1*$^{+/+}$*Stk39*$^{+/+}$RCE and *Oxsr1*$^{fl/fl}$*Stk39*$^{T243A/T243A}$RCE mice was transferred into irradiated RAG1-deficient mice. At least 8 weeks later, the chimeras were treated with tamoxifen on five successive days to delete the floxed exons 9 and 10 of *Oxsr1*, lymph nodes harvested 21 d after start of tamoxifen treatment and *Oxsr1*$^{+/+}$*Stk39*$^{+/+}$RCE or *Oxsr1*$^{-/-}$*Stk39*$^{T243A/T243A}$RCE naive CD4$^+$ T cells purified. (**B**) Abundance of OXSR1 in *Oxsr1*$^{+/+}$*Stk39*$^{+/+}$RCE or *Oxsr1*$^{-/-}$*Stk39*$^{T243A/T243A}$RCE CD4$^+$ T cells was determined by immunoblotting total cell lysates for OXSR1 and ERK2 and normalizing the ratio of OXSR1 to ERK2 to the median value in *Oxsr1*$^{+/+}$*Stk39*$^{+/+}$RCE T cells which was set to 1 (example immunoblot shown below graph) (n = 5). Each point represents a different mouse; horizontal lines indicate median; data shown from 1 experiment representative of 2 independent experiments. Statistical analysis carried out using the Mann-Whitney U test. ** $0.001 < p < 0.01$.

Figure S4

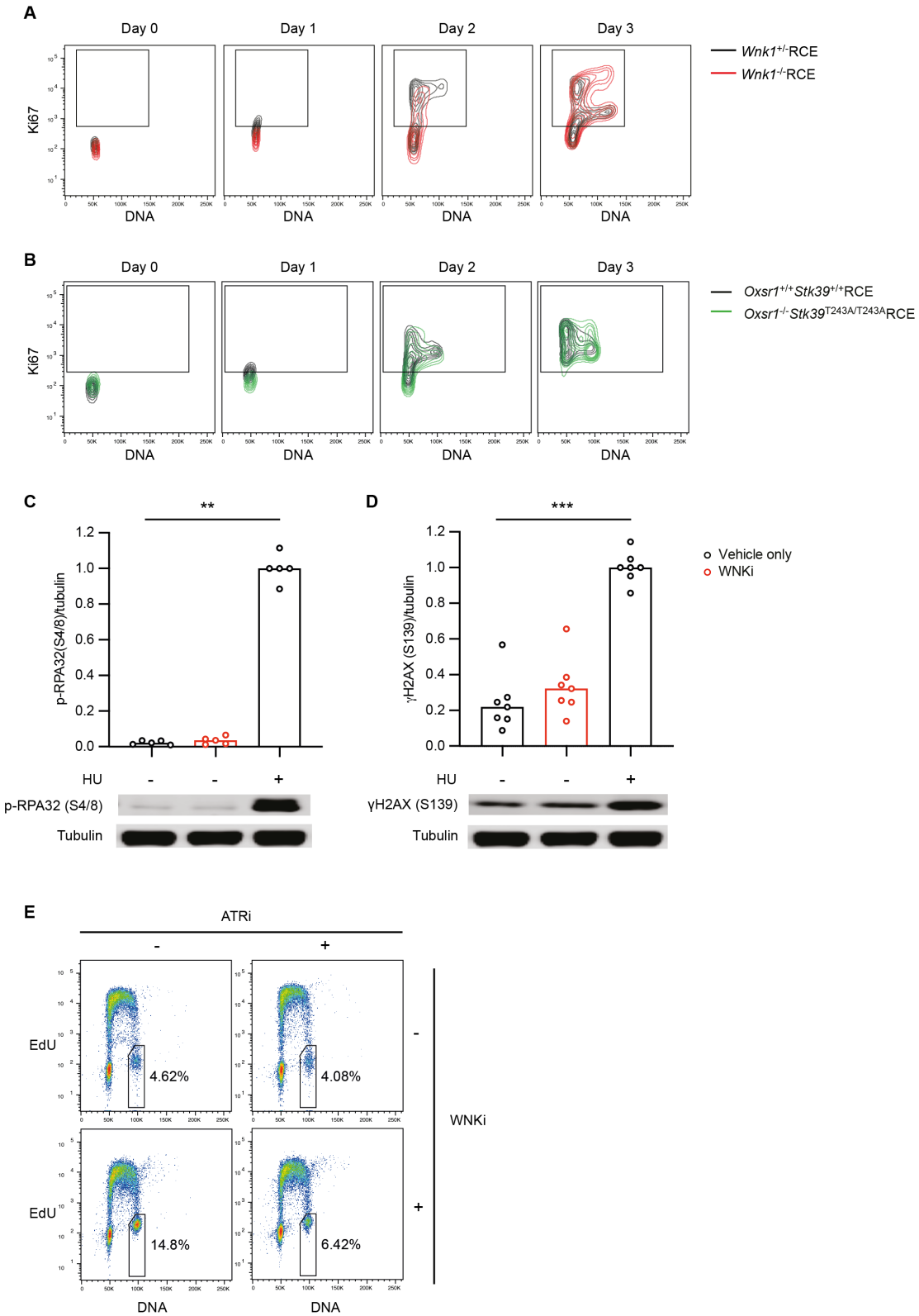
A
Day 0
Day 1
Day 2
Day 3
Ki67
DNA
Wnk1+/-RCE
Wnk1-/-RCE
B
Oxsr1+/+Stk39+/+RCE
Oxsr1-/-Stk39T243A/T243ARCE
C
**
p-RPA32(S4/8)/tubulin
HU
p-RPA32 (S4/8)
Tubulin
D
***
γH2AX (S139)/tubulin
γH2AX (S139)
Vehicle only
WNKi
E
ATRi
EdU
4.62%
4.08%
14.8%
6.42%
WNKi

Figure S4. Delayed TCR/CD28-induced entry into G1 in CD4$^+$ T cells with mutations in *Wnk1*, *Oxsr1* and *Stk39*.

(**A, B**) Example flow cytometric density plots of Ki67 expression and DNA content of CD4$^+$ T cells of the indicated genotypes activated on anti-CD3ε and anti-CD28 antibodies for the indicated times. Gates shown used to identify Ki67$^+$ population. (**C**, **D**) Graphs showing abundance of p-RPA32 (S4/S8) (C) and γH2AX (S139) (D) relative to Tubulin in CD4$^+$ T cells activated on plate-bound anti-CD3ε and anti-CD28 antibodies for 3 d in the presence of WNKi or vehicle only (n=5-7). Where indicated, 4 mM hydroxyurea (HU) was added for the final 2 h of culture. Amounts of p-RPA32 and γH2AX were determined by immunoblotting total cell lysates with antibodies to these phosphorylated proteins and to Tubulin and normalizing the resulting pRPA32/tubulin and γH2AX/tubulin ratios to the median ratio in HU-treated cells which was set to 1. Columns show median; each point represents a single mouse. (**E**) Representative flow cytometric pseudocolor plots of DNA and EdU content of single, live CD4$^+$ T cells activated for 72 h on anti-CD3ε- and anti-CD28-coated cell culture dishes. Cells were treated with WNKi for 72 h or ATRi for 6 h where indicated and pulsed with EdU for the final 30 min of the culture. Gates indicate cells in G2/M used to generate data in Fig. 3M, numbers indicate percentage of cells falling into the gate. Data pooled from 3 independent experiments (C, D). Statistical analysis carried out using Mann-Whitney U test. ** $0.001 < p < 0.01$; ***$0.0001<p<0.001$.

Figure S5

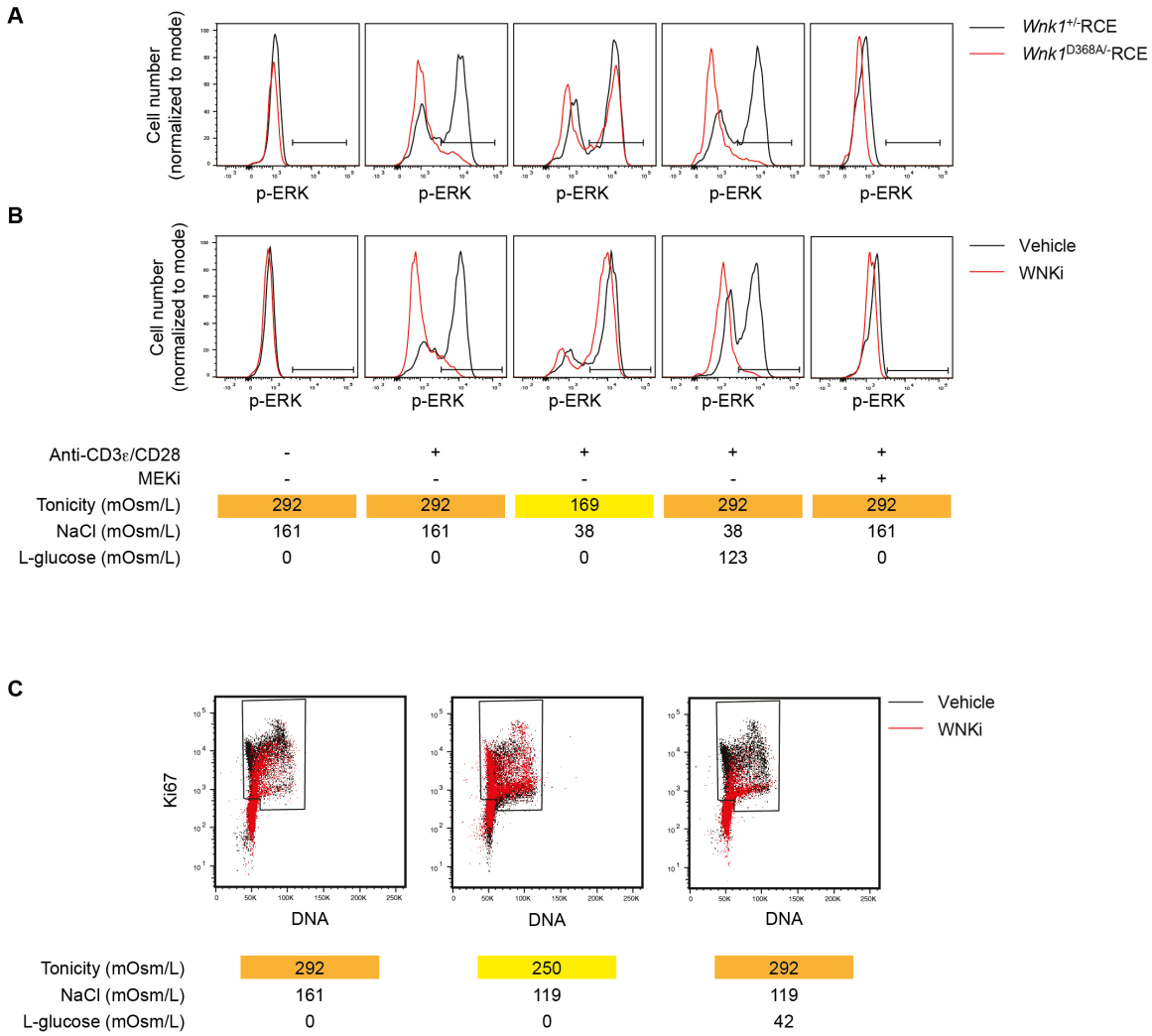

Figure S5. WNK1-dependent water influx is required for TCR signaling and G1 entry. (**A**, **B**) Histograms of phospho-ERK1/2 (p-ERK, T202/Y204) abundance in CD4$^+$ T cells activated for 1 h on plates coated with anti-CD3ε and anti-CD28 antibodies at the tonicities indicated and in the presence of MEKi or vehicle only, measured by flow cytometry. Histograms show a comparison of *Wnk1*$^{+/-}$RCE and *Wnk1*$^{D368A/-}$RCE CD4$^+$ T cells (A) or WT CD4$^+$ T cells treated with WNKi or vehicle (B). Gate indicates p-ERK high cells. (**C**) Example dot plots of Ki67 expression and DNA content of WT CD4$^+$ T cells activated for 2 d on anti-CD3ε and anti-CD28 antibodies in the presence of WNKi or vehicle only at the

tonicities indicated, made by altering NaCl and L-glucose concentrations, measured by flow cytometry; gate indicates $Ki67^{+}$ cells, excluding $Ki67^{-}$ cells in G0.